Comparison of Simulated 2D Temperature Profiles with Time-Lapse Electrical Resistivity Data at the Schilthorn Crest, Switzerland

Jeannette Noetzli
Glaciology, Geomorphodynamics, Geochronology, Geography Department, University of Zurich, Switzerland
Christin Hilbich
Department of Geography, University of Jena, Germany
Christian Hauck
Institute for Meteorology and Climate Research, University of Karlsruhe/Forschungszentrum, Karlsruhe, Germany
Martin Hoelzle
Glaciology, Geomorphodynamics, Geochronology, Geography Department, University of Zurich, Switzerland
Stephan Gruber
Glaciology, Geomorphodynamics, Geochronology, Geography Department, University of Zurich, Switzerland

Abstract

The Schilthorn Crest in the Bernese Alps, Switzerland, is a prominent permafrost research site. Topographic and transient effects influence the temperature field below the east-west oriented crest. Measured T(z)-profiles in boreholes, however, do not provide sufficient information for a comprehensive description of the subsurface temperature distribution. We combine ground temperature measurements, electric resistivity tomography (ERT) monitoring, and numerical modeling to investigate the 3-dimensional thermal regime below the crest. The modeled temperature field of a north-south oriented cross section agrees well with ERT results along the same profile. The simulated thermal regime below the Schilthorn is characterized by generally warm permafrost, with the coldest zone below the upper part of the north-facing slope, and permafrost a little below the surface on the south-facing slope. The combination of temperature modeling and measurements and geophysical monitoring bears potential to improve simulation and validation strategies.

Keywords: alpine permafrost distribution; electrical resistivity; thermal modeling; tomography monitoring; transient and topographical temperature effects.

Introduction

Permafrost was first found on Schilthorn summit, Switzerland, when the facilities for the cable car were built between 1965 and 1967. During the construction of the buildings, several ice lenses with a thickness of up to 1 m were encountered. Since then, extensive research has taken place on Schilthorn (e.g., Imhof 2000, Vonder Muehll et al. 2000, Hauck 2001, Mittaz et al. 2002, Hilbich et al. 2008), making it to one of the most intensively investigated permafrost sites in the European Alps. Three boreholes in perennially frozen ground were drilled within the PACE-project between 1998 and 2001 (Harris 2001). These boreholes provide the basis for monitoring and quantification of changes in the permafrost thermal regime.

In mountain areas, the interpretation of T(z)-profiles measured in boreholes with respect to climate signals is complicated by topographic effects (Gruber et al. 2004). The Schilthorn represents an east-west oriented ridge with a warm south-facing and a colder north-facing slope. Even though measured temperature profiles in boreholes enable an initial assessment of topography related and transient effects, they are only representative of isolated local spots. A comprehensive analysis of permafrost distribution and evolution below the crest can only be achieved by integrating additional subsurface data

Figure 1. View of the Schilthorn Crest in the Bernese Alps looking eastward. The ERT-Profile starts just below the meteo station in the northern slope and reaches across the crest approximately to the southern border of the photo.

In this paper, we combine measurements of surface and subsurface temperatures, electric resistivity tomography (ERT), and numerical modeling of a subsurface thermal field for a 2-dimensional investigation of permafrost conditions below the Schilthorn crest. A 2D heat transfer model is forced by measured near-surface temperatures at the upper boundary to simulate the thermal field of a north-south cross section of the ridge. An ERT monitoring system was installed across the same profile, which provides additional information on subsurface conditions, and enables comparison of modeling results for a qualitative validation.

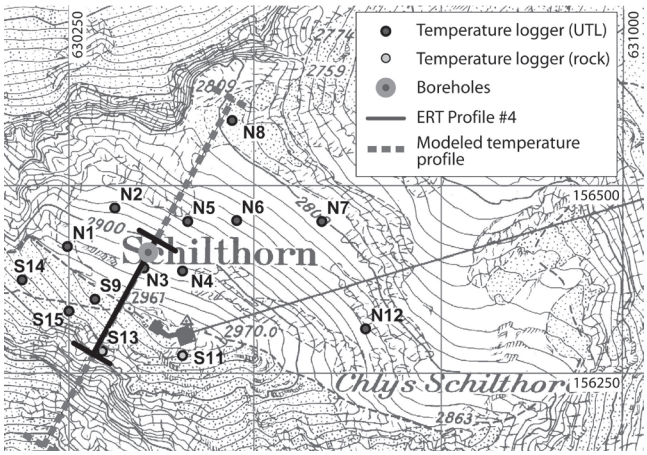

Figure 2. Overview of the field site Schilthorn Crest showing the locations of the near-surface temperature loggers, the boreholes, the measured ERT profile, and the modeled north-south cross section. Map: Swisstopo.

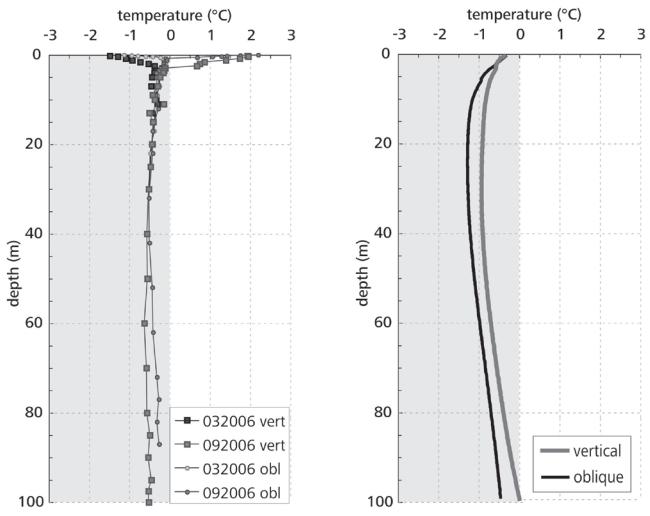

Figure 3. T(z)-profiles for the 101 m vertical (vert, black) and oblique (obl, gray) boreholes on the Schilthorn for spring and autumn 2006 (left). Modeled T(z)-profiles extracted from the temperature field in Fig. 4 at the locations of the two boreholes (right; colored illustration available on CD-Rom).

The Field Site

The Schilthorn (2970 m a.s.l., 46.56°N/7.83°E, Figs. 1, 2) is located in the Bernese Oberland in the Northern Swiss Alps. The three boreholes are located on a small plateau on the north-facing slope approximately 60 m below the summit. Air temperatures recorded at the meteo station close to the boreholes indicate an annual mean of -2.8 °C for the years 1999–2007 (Hoelzle and Gruber 2008). The annual precipitation is estimated to 2700 mm and about 90% of it falls as snow (Imhof 2000). As the precipitation maximum occurs during summer and due to additional snow input through wind transport, the snow cover on the northern slope usually persists from October until June or even July (Hauck 2001). The average snow depth since the beginning of measurements at the meteo station in 1999 is around 80 cm. The Schilthorn consists of dark micaceous shales that weather to form a fine-grained debris layer of up to several meters in thickness covering the entire summit region. The ice content of the subsurface material is assumed to be generally low (around 5–10% in the upper meters, as reported from direct observations, Imhof et al. 2000, Vonder Mühll et al. 2000).

Temperature Measurements

Boreholes

In the scope of the PACE project, a 14 m borehole was drilled in 1998 and complemented by two 101 m boreholes in 2000. Today, these boreholes are part of the Permafrost Monitoring Switzerland (PERMOS). The deeper boreholes were drilled vertical and with an angle of 60° to the vertical in order to account for topography-related effects. Temperatures measured in these boreholes point to warm permafrost conditions with temperature values between -1 and 0°C below depth of the zero annual amplitude (ZAA) at approximately 20 m, and to a very small temperature gradient with depth (Fig. 3, left). The temperature gradient in the oblique borehole is slightly greater than in the vertical borehole. Ground temperatures are considerably higher compared to other sites at similar altitude and exposition, which is probably due to the low bedrock albedo, thick snow cover, and low ice content at the site (Hauck 2001).

Ground surface temperatures

In addition to the borehole measurements, 14 temperature loggers were distributed on both sides of the crest in summer 2005 and 2006 to measure near surface-temperatures (see Fig. 2). The loggers were installed at a depth of 30 cm (UTL mini loggers) and 10 cm (rock temperature loggers), respectively, and temperatures are recorded every 2 hours. The accuracy of the temperature loggers is given as ±0.25°C and ±0.1°C, respectively. As the lower parts of the steep southern slope are difficult to access, loggers were only placed in the upper part of the slope. These near-surface temperature measurements provide the upper boundary condition for the numerical heat transfer model presented in the following section. In addition, they can be used to constrain the interpretation of the geophysical results concerning the subsurface thermal regime.

Numerical Modeling of Subsurface Temperatures

General approach

We considered a purely conductive transient thermal field under variable topography in an isotropic and homogeneous medium according to Carslaw and Jaeger (1959). In steep topography, heat transfer at depth mainly results from conduction, driven by the temperature variations at the surface. Processes such as fluid flow are not included in this first step. Subsurface temperatures are calculated for conditions in the hydrological year 2006/2007 (i.e., 1 Oct. to 30 Sept.) based on mean annual conditions at the surface. That is, seasonal variations at the surface are not included, and temperature variations above the ZAA are not simulated.

Ice contained in the pore space and crevices delays the

response to surface warming by the uptake of latent heat during warming. This is addressed in our finite-element heat transport model by apparent heat capacity, which substitutes the volumetric heat capacity in the heat transfer equation and includes energy consumed during phase change. We used the approach described by Mottaghy & Rath (2006).

The resulting temperature pattern is expected to be similar for any north-south oriented cross crest profile. Hence, simulations are conducted for a 2D section across the crest and the borehole site on the northern slope. The assumption of symmetry in an east-west direction is supported by first results of a quasi-3D geoelectrical investigation including four parallel and two orthogonal ERT-profiles in the Schilthorn summit area (Krauer 2008). The selected profile was extracted from a digital elevation model (DEM) with 10 m horizontal resolution (Data Source: Swissphoto). The finite element (FE) mesh was generated for this geometry with corresponding 10 m resolution at the surface, and lower resolution at greater depth. The mesh consists of 1468 elements. The software package COMSOL Multiphysics was used for forward modeling of subsurface temperatures.

Boundary conditions

For all near-surface temperature loggers the mean annual temperature for the hydrological year 2006/2007 was calculated and set as an upper boundary condition at the corresponding elevation and side of the modeled profile. The measured thermal offset between the ground surface and TTOP is small at Schilthorn (about 0.3°C; cf. Hoelzle & Gruber 2008) and is, hence, neglected in the simulations.

The years 2006 and 2007 were very warm and clearly above the long-term average. Therefore, measured near-surface temperatures are not representative for the thermal conditions at the surface during the past decades and century. Transient effects are likely to occur and, therefore, initialization of the heat conduction model is required in order to perform a realistic simulation of the current subsurface temperature field. Based on the assumption that surface temperature fluctuations mainly follow air temperatures, we used mean annual air temperatures (MAAT) from the meteo station on Jungfrauoch (3576 m a.s.l., Data source: MeteoSwiss) some 10 km east of Schilthorn to describe the evolution of the upper boundary. For Jungfraujoch, air temperature data is available back to 1933. The total difference in MAAT between 2006 and the mean of the period 1933–1950 is +1.52°C. We additionally assumed a difference in air temperature of +0.5°C between the start of the data recordings and the Little Ice Age (ca. 1850). The model initialization was started in 1850, and daily time steps were taken. A uniform lower boundary heat flux of 0.08 W m^{-2} was set at sea level, and thermal insulation was assumed for the lateral boundaries of the geometry.

Subsurface properties

Subsurface material properties were assigned on the generated FE mesh. In purely diffusive and transient simulations, thermal conductivity, volumetric heat capacity, and the ice/water content are the petrophysical parameters of importance. However, only little is known on the subsurface characteristics below steep topography and the parameters were set based on published values: Thermal conductivity was assumed as 2.5 W K^{-1} m^{-1}, and heat capacity to 2.0 x 10^6 J m^{-3} K^{-1} for the bulk material (Cermák & Rybach 1982).

Based on estimations from geophysical measurements (cf. Hauck et al. 2008) for the upper layers, a uniform ice content of 5% for the entire profile was assumed in the model simulations. The unfrozen water content is described by an exponential function, and the steepness factor was set to 0.2 (cf. Mottaghy & Rath 2006).

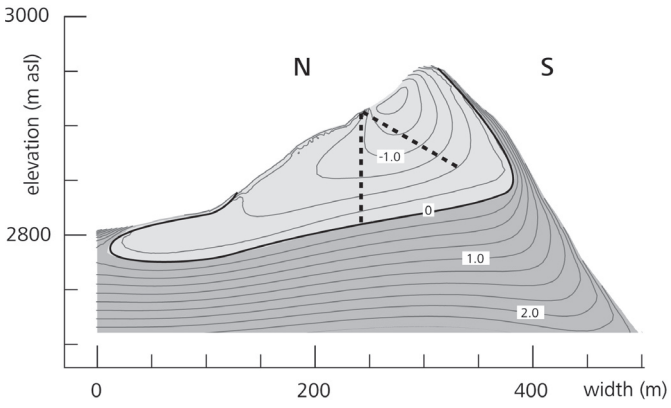

Figure 4. Isotherms of the modeled subsurface temperature field for a north-south cross section of the Schilthorn crest. The 0°C isotherm is depicted in black, and the dashed black lines indicate the boreholes. Light gray areas are permafrost, darker shaded areas are outside permafrost (colored illustration available on CD-ROM).

Modeling results

The resulting temperature field for the Schilthorn profile is depicted in Figure 4. Maximum permafrost thickness amounts to roughly 100 m below the northern slope and the top of the crest. Isotherms are steeply inclined in the top part, and a lateral heat flow exists from the warm south to the colder north face. Simulated permafrost temperatures are higher than -2°C for the entire profile.

The coldest temperatures exist below the northern and central part of the ridge. The reason is that coldest surface temperatures are found in the steep part of the northern slope (mainly due to reduced solar radiation and longer snow cover duration), and that surface temperatures are higher on the small plateau where the boreholes are located, as well as on the southern side. The southern slope is mainly permafrost-free at the surface. However, due to the cold, northern slope permafrost can be found below the surface. In addition, this is caused by the fact that 20th century warming has not yet penetrated to greater depth in the model, which lowers the temperatures a few tens of meters below the surface compared to present-day steady-state conditions. Similarly, permafrost remains below the surface at the foot of the northern slope. These results point to the importance of transient 2D/3D modeling, as such transient and topography related effects could not be detected using steady state 1D models.

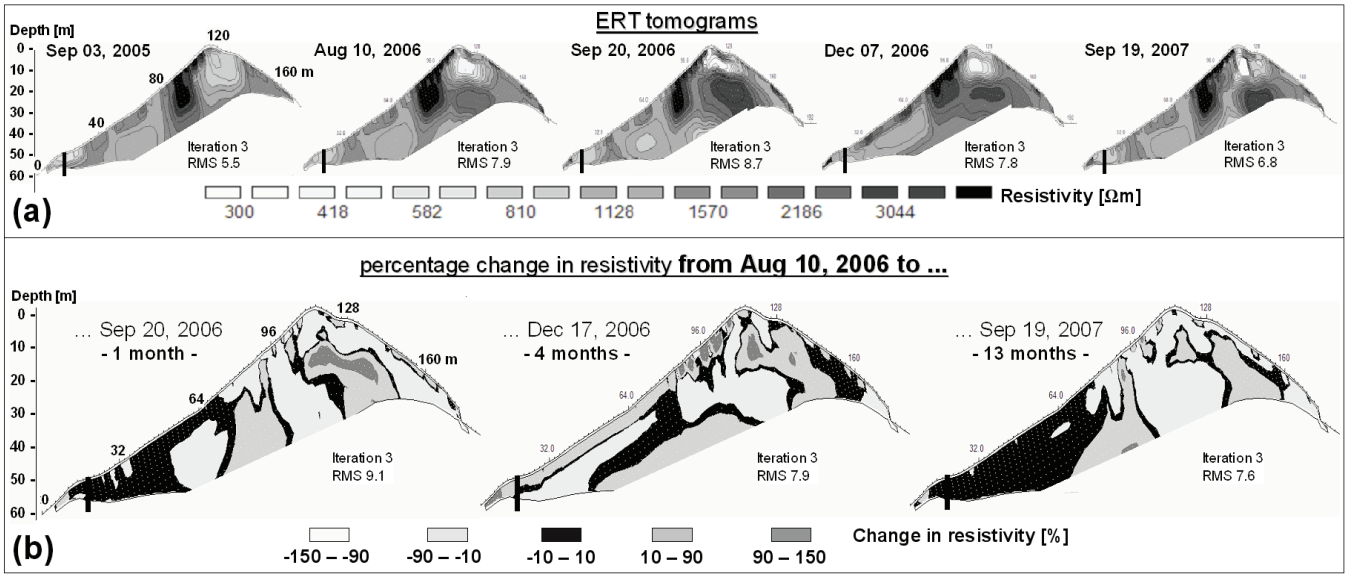

Figure 5. ERT monitoring data illustrated as individual resistivity tomograms for subsequent measurements (a), and as calculated change in resistivity based on the reference profile from August 10, 2006 over one, four, and 13 months (b; colored illustration available on CDRom).

In contrast to ERT profiles (c.f. next section), which mainly allow for a qualitative validation of the general pattern of temperature distribution, comparison with extracted T(z)-profiles at the locations of the boreholes shows the accuracy of the modeled temperature values (Fig. 3). In general, the modeled profiles correspond to the measured data in Figure 3 as temperatures are below -1.5°C for the entire profile, and temperature gradients with depth are small. For both measured and modeled profiles, the oblique borehole shows a slightly more curved profile. However, temperatures of the modeled profile average about 0.2°C colder than the measured values, but range up to 1°C in the upper half of the profile. Further, in the lower parts, the oblique profile is warmer than the vertical profile, which could not be reproduced in the simulation. The results are encouraging given the model error sources, which include: (1) subsurface properties (i.e., ice content, thermal conductivity) are assumed as homogenous for the entire profile and are hardly known at depth; (2) the temperature evolution at the surface may be influenced by effects of solar radiation and snow cover, and, hence, not exactly follow air temperature. In addition, the higher ice content in the limestone scree in the upper meters can slow down the reaction of the subsurface to changing surface temperatures by the uptake of latent heat; (3) small scale variability at the site may cause random errors in logger measurements, and (4) processes such as heat transport by convection are not taken into account.

Geophysical Measurements

Electrical Resistivity Tomography (ERT)

In 1999, a semi-automatic ERT monitoring system was installed on a 60 m line close to the three boreholes in the north facing slope to observe subsurface resistivity changes with respect to ground ice and water content (Hauck 2001, Hilbich et al. 2008). In summer 2005, a second ERT monitoring line (188 m) was installed across the crest, complemented by a quasi-3D ERT survey along four transects across the crest in 2006. Datasets across the crest can be used to analyze the 3D permafrost distribution.

The measured signal is sensitive to temporally variable properties such as temperature, via the unfrozen water, and ice content, as well as unchanging material characteristics, such as lithology and porosity. Repeated ERT measurements, therefore, yield information on the changes occurring in the physical properties of the ground with changing temperature and time (Fortier et al. 1994).

ERT monitoring data of the cross-crest profile (Fig. 2) are available on different time scales: (a) annual measurements in late summer (August/September) for 2005, 2006, and 2007, and (b) seasonal-scale measurements between August and December 2006. Whereas the annual resolution provides interannual resistivity changes between 2005 and 2007, the seasonal scale helps to identify zones with pronounced resistivity changes to delineate ice-free from ice-rich regions. ERT data were processed with the software RES2DINV (Loke & Barker 1995). Besides a qualitative comparison of individual tomograms, a so-called time-lapse inversion of time series of ERT data allows for a quantitative assessment of the resistivity changes.

Results

Figure 5 shows the results of the ERT monitoring across the Schilthorn Crest. In general, measured resistivities are quite low compared to other permafrost sites and do not exceed 4000 Ωm. This is mainly due to the thick fine-grained debris layer covering the summit region. Outcrops of the underlying bedrock also indicate strongly weathered conditions of the micaceous shales with crevices, where water can percolate. In addition to the comparably conductive host material, the low ice content is in accordance with the low resistivity values.

A number of features can be observed in all tomograms (cf. Fig. 6): (A) a relatively homogeneous zone with resistivities between 700 and 1600 Ωm in the lower part of the northern slope, (B) a high resistive zone (>3000 Ωm) in the upper part of the northern slope, (C) a homogeneous intermediary zone in the southern slope with resistivities from 1200 to 1700 Ωm, and (D) a very low resistive anomaly (<500 Ωm) with an underlying high resistive anomaly (>2300 Ωm) at the summit.

The high resistive anomaly in the northern slope (B) may indicate the presence of ground ice and/or firm bedrock. Both possibilities would result in increased resistivity values compared to regions with lower ice contents or more weathered bedrock occurrences, respectively. The low resistive anomaly at the crest (D) is difficult to interpret. In comparable terrain, such low resistivity values are normally associated with very high amounts of unfrozen water or conductive man-made structures (e.g., cables). The presence of such a large amount of water is very unlikely since the crest consists of firm bedrock without a superficial debris cover, whereas metallic remnants from the construction of the summit station (e.g., anchors) are found all over the crest. A man-made low resistive anomaly can therefore, not be excluded. The high resistive anomaly directly below this feature is believed to be an inversion artifact, which is often generated during inversion below a zone of anomalously high or low resistivity values (Rings et al. 2007).

Apart from the high and low resistive anomalies close to the crest, the characteristics of the northern (A) and southern (B) slope seem to be similar. From the qualitative analysis of the individual tomograms no clear indication of differences in permafrost occurrence and ice content between the two slopes is apparent. Calculating the percentage change of resistivities between subsequent measurements (Fig. 6), the tomograms can be transferred into information on seasonally changing properties. From this, zone (A) in the northern slope can be seen as a region with little change in the deeper parts but with pronounced resistivity changes within the upper 4–5 m. This clearly indicates the presence of permafrost with active layer freezing in winter. The deeper parts tend to exhibit slightly lower resistivities in winter, which we interpret as delayed advance of the summer heating (increasing unfrozen water content and therefore decreasing resistivities) into the ground. Zone (B) only yields systematic resistivity changes near the surface, that can be attributed to thawing (decreasing resistivities) between August and September and freezing (increasing resistivities) processes until December. Both processes are similar to the features in zone (A) but seem to be more pronounced. Zone (C) is characterized by a homogeneous resistivity decrease during summer, but shows almost no changes between August and December, i.e., no active layer freezing can be observed. In contrast to the very similar absolute resistivity values, seasonal changes are different in the northern and southern slope. This can be related to differences in subsurface material properties, i.e., permafrost or ice content.

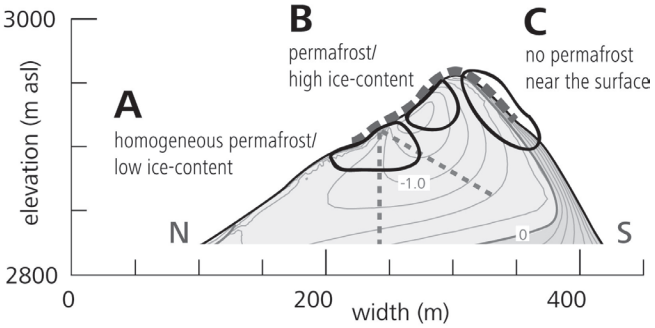

Figure 6. Three features that are addressed in the discussion section are highlighted by black circles: (A) A homogeneous permafrost zone in the lower northern slope with low ice content, (B) a cold zone in the north slope with a high ice content, and (C) no permafrost near the surface on the southern slope. Additionally, grey dashed lines indicate the boreholes and the extent of the ERT profile (colored illustration available on CD-ROM).

Discussion

In both the modeled temperature field and the ERT profiles, three zones in the investigated cross section of the Schilthorn Crest can be distinguished that are particularly interesting (Fig. 6). Cross validation of the results of the two complementary approaches enables an interpretation as follows.

(A) In the lower part of the northern slope, a zone of homogeneous temperatures and resistivities exits. The small variations in temperature in this area may be explained by the fact that temperature values are only little below the melting point and the energy input of the recent warming is consumed by latent heat. Also, the results from ERT monitoring suggest high amounts of unfrozen water and only little ice content (Hauck et al. 2008).

(B) In the upper part of the northern slope a zone of cold temperatures exists. The corresponding zone of high resistivity in the ERT profile is, hence, probably caused by higher ice content rather than by geological characteristics. This is also supported by the larger seasonal resistivity changes pointing to higher contents of ice and unfrozen water than in the lower part of the northern slope.

(C) The permafrost boundary on the southern slope is likely situated only a little below the surface, an effect that can be mainly attributed to surface warming of the past century that has not yet affected greater depths. Seasonal resistivity changes support the hypothesis that there is no permafrost near the surface in the southern slope.

The results of this qualitative validation corroborate the assumption that the general pattern of the subsurface temperature field can be modeled using diffusive and transient 2D and 3D simulations. Using such an approach enables the simulation of temperature fields at greater depths that cannot be reached by geophysical measurements or direct measurements in boreholes. Additionally, the numerical model can be used to calculate scenarios of the evolution of subsurface temperatures and of future permafrost occurrence below the Schilthorn Crest by prescribing the evolution of

the upper boundary condition or by coupling the model to a surface energy balance model and/or using regional climate model output (cf. Noetzli et al. 2007).

Conclusions and Perspectives

The subsurface thermal field of a 2D-section across the Schilthorn was modeled assuming a purely conductive and homogenous underground in a first approach. Comparison with measured ground temperatures and ERT profiles leads to the following conclusions:

- The subsurface thermal regime of the Schilthorn Crest is predominantly influenced by both topography and transient effects. The cold northern slope and the recent 20th century warming induce permafrost on the southern side of the crest only a little below the surface.
- The thermal regime of the profile can be characterized by a cold zone below the upper part of the northern slope, permafrost occurrence only a little below the surface on the southern slope and in the lowest part of the northern slope, and rather homogeneous conditions at and below the area of the boreholes.
- The modeled temperature field agrees with the results from ERT monitoring. The three zones mentioned above can be distinguished in the results of both methods.

ERT monitoring on Schilthorn is being continued in the scope of PERMOS. The combination of thermal modeling, temperature measurements in boreholes and geophysical surveys bears potential to further improve modeling and validation strategies. These may include (1) quantitative comparison of numerical results and measured data to estimate model performance, (2) extending single point temperature data to larger scales using 2D or 3D resistivity values, and (3) improving the representation of the subsurface physical properties in the model by incorporating subsurface information (e.g., geological structures, water/ice content) detected by geophysical surveys.

Acknowledgments

We are indebted to Michael Krauer for making available the ERT data measured within his M.S. thesis. Further, we'd would like to thank the motivated students that helped us in the field and the Schilthornbahnen AG for generous logistic support. Part of this study (JN) was financed by the Swiss National Science Foundation as part of the NF 20-10796./1 project, and geophysical fieldwork (CH) was partly financed by PERMOS.

References

Carslaw, H.S. & Jaeger, J.C. 1959. Conduction of heat in solids. In *Oxford Science Publications*. Oxford: Clarendon Press, 510 pp..

Cermák, V. & Rybach, L. 1982. Thermal conductivity and specific heat of minerals and rocks. In G. Angeneister, (ed.), *Landolt-Börnstein Zahlenwerte und Funktionen aus Naturwissenschaften und Technik, Neue Serie, Physikalische Eigenschaften der Gesteine*. V/1a. Berlin: Springer Verlag, 305-343

Gruber, S., King, L., Kohl, T., Herz, T., Haeberli, W. & Hoelzle, M. 2004. Interpretation of geothermal profiles perturbed by topography: The Alpine permafrost boreholes at Stockhorn Plateau, Switzerland. *Permafrost and Periglacial Processes* 15(4): 349-357.

Fortier, R., Allard, M. & Seguin, M.K. 1994. Effect of physical properties of frozen ground on electrical resistivity logging. *Cold Regions Science and Technology* 22: 361-384.

Harris, C., Haeberli, W., Vonder Muehll, D., & King, L. 2001. Permafrost monitoring in the high mountains of Europe: The PACE project in its global context, *Permafrost and Periglacial Processes* 12: 3-11.

Hauck, C. 2001. *Geophysical methods for detecting permafrost in high mountains*. Ph.D. Thesis. Zürich, Switzerland: ETH-Zürich, 204 pp.

Hauck, C., Bach, M. & Hilbich, C. 2008. A 4-phase model to quantify subsurface ice and water content in permafrost regions based on geophysical datasets. *Proceedings of the Ninth International Conference on Permafrost, Fairbanks, Alaska, June 29–July 3, 2008* (this proceedings).

Hilbich, C., Hauck, C., Hoelzle, M., Scherler, M., Schudel, L., Völksch, I., Vonder Mühll, D. & Mäusbacher, R. 2008. Monitoring of mountain permafrost evolution using electrical resistivity tomography: A seven-year study of seasonal, annual and long-term variations at Schilthorn, Swiss Alps. *Journal of Geophysical Research* 113:F01S90, doi:10.1029/2007JF000799.

Hilbich, C., Hauck, C., Delaloye, R. & Hoelzle, M. 2008. A geoelectric monitoring network and resistivity-temperature relationships of different mountain permafrost sites in the Swiss Alps. *Proceedings of the Ninth International Conference on Permafrost, Fairbanks, Alaska, June 29–July 3, 2008* (this proceedings).

Hoezle, M & Gruber, S. 2008. Borehole measurements and ground surface temperatures and their relationship to meteorological conditions in the Swiss Alps. *Proceedings of the Ninth International Conference on Permafrost, Fairbanks, Alaska, June 29–July 3, 2008* (this proceedings).

Imhof, M. 2000. Permafrost investigation in the Schilthorn massif, Bernese Alps, Switzerland. *Permafrost and Periglacial Processes* 11(3): 189-206.

Krauer, M. 2008. Versuch einer 3-dimensionalen Erfassung des Peramfrosts in der Gipfelregion des Schltohrns mittels Geoelektrik, M.S. Thesis. University of Zurich, 112 pp.

Loke, M.H. & Barker, R.D. 1995. Least-squares deconvolution of apparent resistivity. *Geophysics* 60: 1682-1690.

Mottaghy, D. & Rath. V. 2006. Latent heat effects in subsurface heat transport modeling and their impact on paleotemperature reconstructions, *Geophysical Journal International* 164: 236-245.

Noetzli, J., Gruber, S., Kohl, T., Salzmann, N. & Haeberli, W. 2007. Three-dimensional distribution and evolution of permafrost temperatures in idealized high-mountain topography. *Journal of Geophysical Research* 112: doi:10.1029/ 2006JF000545.

Rings, J., Preko, K., Scheuermann, A. & Hauck, C. 2007. Soil water content monitoring on a dike model using electrical resistivity tomography. *Near Surface Geophysics* (in press).

Stocker-Mittaz, C. 2002. *Permafrost distribution modeling based on energy balance data*. Ph.D Thesis. Zurich, Switzerland: University of Zurich, 122 pp.

Vonder Mühll, D., Hauck, C. & Lehmann, F. 2000. Verification of geophysical models in Alpine permafrost by borehole information. *Annals of Glaciology* 31: 300-306.